REVIEW

Materials interface engineering for solution–processed photovoltaics

Michael Graetzel[1], René A. J. Janssen[2], David B. Mitzi[3] & Edward H. Sargent[4]

Advances in solar photovoltaics are urgently needed to increase the performance and reduce the cost of harvesting solar power. Solution-processed photovoltaics are cost-effective to manufacture and offer the potential for physical flexibility. Rapid progress in their development has increased their solar–power conversion efficiencies. The nanometre (electron) and micrometre (photon) scale interfaces between the crystalline domains that make up solution-processed solar cells are crucial for efficient charge transport. These interfaces include large surface area junctions between photoelectron donors and acceptors, the intralayer grain boundaries within the absorber, and the interfaces between photoactive layers and the top and bottom contacts. Controlling the collection and minimizing the trapping of charge carriers at these boundaries is crucial to efficiency.

One hundred and twenty thousand terawatts of solar power irradiate Earth. Globally, humans consume only 15 terawatts. Solar power is abundant, free and can be harvested with minimal effect on the environment.

The cost and efficiency of the solar cells that make use of this power are of paramount importance. Single-crystal solar cells are formed from a continuous piece of crystal, but solution-processed photovoltaics are manufactured on large, potentially flexible substrates (Fig. 1). Light-absorbing and electrode materials are applied to the substrate by techniques such as blade coating, spray coating, printing and slot-die coating. Many solution-processing approaches use low temperatures, reducing the energy cost associated with solar-cell manufacturing and therefore the energy payback time. Lightweight, flexible solar modules can also lower the installation and maintenance costs.

Four main families of solution-processed solar technologies are approaching or have exceeded 10% solar-power conversion efficiency. The challenge now is to continue this progress. Advances rely on controlling the abundant materials interfaces that make up these highly nanostructured devices. In this Review, we discuss the chemistry, physics and materials science of these interfaces, and their control through materials chemistry. In particular, we focus on dye-sensitized solar cells (DSSCs)[1], organic photovoltaics[2], solution-processed bulk inorganic photovoltaics[3] and colloidal quantum-dot[4] solar cells.

The charge-separating junction is the boundary between two intimately contacted materials at which photogenerated electron–hole pairs are separated into longer-lived charge carriers (Fig. 2a, b). Efficient operation of the solar cell relies on the separation and collection of energy-bearing photocarriers before they lose their excess energy through recombination. Typical diffusion lengths for the performance-limiting photocarrier — minority charge carriers — are within the 5–500-nm range in solution-processed semiconductors, but the absorber thickness required to achieve complete absorption of solar irradiation of interest is often considerably more than this. This results in a possible trade-off between electron extraction and optical absorption if a planar absorber is used. To break this compromise, solution-processed solar cells make use of highly nanostructured and mesostructured interfaces.

Solution-processed photovoltaic materials generally contain significant degrees of disorder, often because of the boundaries that define the randomly orientated crystalline domains in both organic and inorganic semiconductors. Transport within these domains, as well as at their boundaries (including transport-limiting mechanisms, such as charge-carrier trapping), requires attention and optimization.

One example of a beneficial boundary effect is the quantum confinement of charge carriers to well-defined nanocrystalline domains, such as in semiconductor quantum dots. This effect allows the tuning of energy levels in materials. Wide-ranging tuning is advantageous because the Sun emits such a broad spectrum of light (Fig. 2c). Relying on one absorber bandgap limits the solar-cell power-conversion efficiency to 31% (ref. 5), whereas stacking cells with different bandgaps to create multijunction configurations could increase the power-conversion efficiencies to, in principle, a 68% limit (Fig. 2d).

We present the benefits of structured charge-separating interfaces and review the chemical management of their electronic properties, discuss interfaces within light-absorbing materials, describe the management and characterization of these interfaces, and summarize the progress and prospects in the field.

Morphology of charge–separating interfaces

DSSCs[6] (Fig. 3a) illustrate the use of nanostructured materials to overcome weak absorption. A monolayer of sensitizer molecules is anchored, with a linker, to an electron-accepting large-bandgap semiconductor such as titanium oxide, tin oxide or zinc oxide. If the monolayer was tethered to a planar electrode, it would absorb an insignificant fraction of solar radiation (less than 1%). Instead, because the electrode has a high-contact area, a three-dimensional junction is formed with the metal-oxide nanoparticles. This nanostructured electrode is many micrometres thick, and the dye–nanoparticle interface is more than a thousand times the area of the solar cell.

Interfacial considerations are of particular concern in an architecture in which every absorber molecule also forms one side of the charge-separating junction. Four interfacial electron-transfer reactions have a pivotal role in the efficiency of photoinduced charge separation. Injection of electrons from the dye into the conduction band of the oxide nanoparticles must proceed faster than exciton recombination within the dye. Recombination of forward-injected photoelectrons across the dye–electrode interface must be prevented. The sensitizer must be regenerated by donation of electrons from the electrolyte. Finally,

[1]Institute of Photonics and Interfaces, Swiss Federal Institute of Technology, CH-1015 Lausanne, Switzerland. [2]Molecular Materials and Nanosystems, Eindhoven University of Technology, PO Box 513, 5600 MB Eindhoven, The Netherlands. [3]IBM TJ Watson Research Center, Yorktown Heights, New York 10598, USA. [4]Department of Electrical and Computer Engineering, University of Toronto, Toronto, M5S 3G4, Canada.

recombination must be eliminated in the electrolyte or hole conductor. Through the molecular engineering of sensitizers, quantum yield values have exceeded 80% across the entire visible and near-infrared spectral range[7].

In organic solar cells, a mixture of semiconductors forms a bulk heterojunction[8,9] (Fig. 3b), again creating a large donor–acceptor interfacial area. The excitons generated through light absorption in the donor diffuse to a heterointerface with the acceptor, where they dissociate into weakly bound charge-transfer states or free carriers. These then need to be separated from the interface and transported to contacts through percolating paths within the distinct electron- and hole-transporting phases. This sequence of steps is affected by the morphology of the active layer. To optimize performance, intimate donor–acceptor interpenetration in the photoactive layers creates a large interface, resulting in a high quantum yield of exciton dissociation; these domains should be large enough to allow rapid charge separation and transport from the interface to prevent recombination[10]. Molecular ordering within materials and controlled phase segregation among the components enhance power-conversion efficiency.

The morphology that is needed to optimize performance is established during the formation of organic films. Solvent choice and drying, and processing additives, determine the nature and extent of the phase segregation. Post-deposition treatments such as thermal annealing may have a role in creating and stabilizing the nanoscale interpenetrating network of materials. For blends of poly(3-hexylthiophene) (P3HT) with the C_{60} fullerene derivative phenyl-C61-butyric acid methyl ester (PCBM) (Fig. 4a, b), both can be rendered semicrystalline. With annealing, P3HT forms long, thin conducting nanowires in a more homogeneous nanocrystalline PCBM film[11]. Increased phase separation and crystallization have a profound effect on the photophysical and transport properties of the active layer.

This insight has been gained through combined experimental and model-based analysis, such as electron tomography with optoelectronic modelling[12], and has led to the three-dimensional visualization of the bulk heterojunction, with implications for device performance (Fig. 4a). Bright-field transmission electron microscope (TEM) morphology observation and acquisition of a series of different tilt angles were combined and iteratively reconstructed to form three-dimensional TEM images, establishing the distance from each volume of donor material to the nearest location of acceptor material, known as the spherical contact distances. This determined the distribution of probability, assessed throughout the volume of a blended film, that an exciton generated inside the donor will find the acceptor at a certain distance. For excitons with a diffusion length of about 10 nm, the calculated exciton quenching efficiency was obtained for each sample, and the results showed that exciton quenching was much more efficient in materials with a finer bulk heterojunction morphology.

Colloidal quantum-dot solar cells (Fig. 3c) are also limited by the diffusion lengths of minority carriers (10–100 nm)[13,14], which are shorter than their above-bandgap optical absorption lengths (100–1,000 nm). They could also benefit from high interfacial areas. By moving beyond planar geometries, photocurrents have been increased because of the enhanced volume of depleted colloidal quantum-dot material from which electric-field-induced drift transport efficiently extracts photocharges[15]. In light of this, the optimal pore size is in the same range as the depletion-region thickness (150–200 nm). Because a continuous semiconductor phase of quantum dots rather than a monolayer of dye is used, the need for an abundant surface area is reduced compared with DSSCs, so columnar electrodes can be deployed[16].

Solution-processed copper-indium-gallium-selenide (CIGS) and copper-zinc-tin-sulphide (CZTS) semiconductors (Fig. 3d) form, with heat treatment, polycrystalline semiconductor films made up of large (micrometre-sized) single-crystal grains. As a result, electron and hole mobility can enter the 10–100 $cm^2 V^{-1}s^{-1}$ range, avoiding the need for bulk heterojunction analogues. In this case, planar interfaces are highly effective.
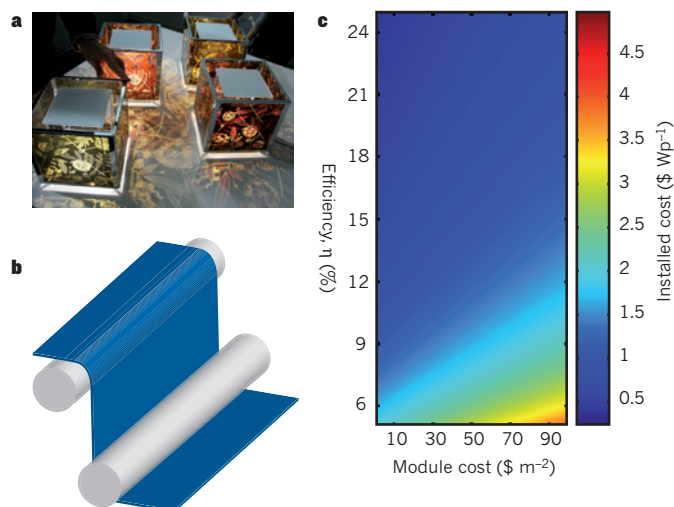
Figure 1 | Solution-processed photovoltaics. a, Commercial dye-sensitized solar cells illustrate the production of photovoltaic technologies through printing. During the day, the cells harvest light from the Sun or ambient light in a room, and in the evening the stored energy can be used for decorative illumination. Image courtesy of S. Uchida, University of Tokyo. **b,** Using a roll-to-roll technique to manufacture solution-processed solar cells reduces the manufacturing, deployment and energy costs involved. **c,** The installed cost per Watt-peak (Wp) as a function of module cost and module efficiency, assuming that balance-of-systems costs can be reduced to US$100 per square metre. Once the module cost is known and the efficiency determined, the installed cost can be established.

Electronics of charge–separating interfaces

When the interfacial area is maximized, the chemistry and resultant electronics of donor–acceptor interfaces become particularly important. On the positive side, the forward injection of charge carriers into the acceptor is helped by the abundance of sites available, but back recombination of the charge-separated carriers across the interface becomes more likely. Technical advances have highlighted the opportunities to manage the crucial charge-separating interface using materials chemistry.

In DSSCs, the light-absorbing dye molecules are anchored to the oxide nanoparticle electrode through coordinative bonding of the linker to the metal ions exposed at the surface of the metal oxide. Carboxylate and phosphonate groups are particularly effective as linkers. Forward transfer is determined by the energetic position of the lowest unoccupied molecular orbital (LUMO) level of the sensitizer compared with the conduction band of the acceptor, and the strength of electronic coupling between the initial and final states associated with the transfer. Engineering these two aspects has led to electron injection efficiencies approaching unity. Systematic investigations[17] of the dynamics of electron injection for perylene-carboxylic-acid-sensitized titanium-oxide nanocrystals have shown that forward injection proceeds with about a 13 fs time constant, which is consistent with theoretical predictions. Adding a saturated -CH2-CH2- spacer between the chromophore and the carboxylate anchoring group extended the injection time to 57 fs, confirming the strong distance dependence of the electron transfer rate. By contrast, introducing an unsaturated -CH=CH- did not alter the electron injection time, as a result of the enhanced electronic coupling through the double bond.

Recombination across the phase boundary that separates the electron- and hole-conducting media is the reverse of forward injection, and lowers the net quantum yield. Avoiding this requires engineering of the interface to impede the backflow of electrons across the junction. The sensitizer slows down the interfacial charge recombination by forming a dense self-assembled monolayer. This also occurs with infilling, using co-adsorbents at the oxide interface. This improved rectification benefits the open-circuit voltage and results in a higher net charge collection efficiency by ensuring that forward transfer is
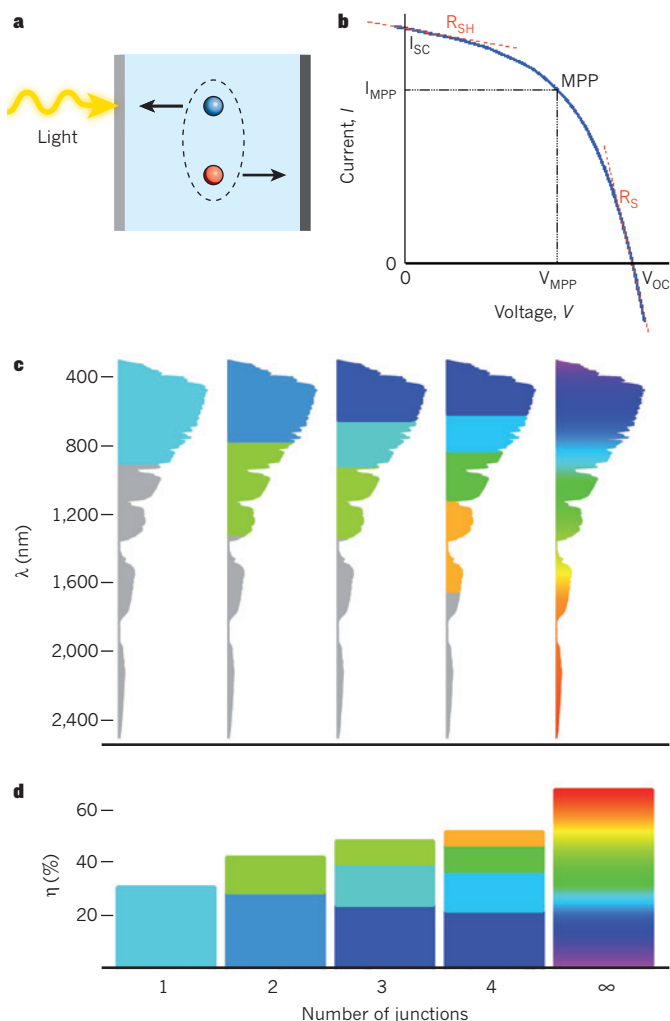
Figure 2 | Photovoltaic principles and performance. a, Light absorbed by the dye, polymer or inorganic semiconductor creates an excited photocarrier that quickly thermalizes to the band edge. Efficient solar cells extract the photocharge before it recombines. **b,** Solar cells must transfer power to load. Their operating current at the maximum power point multiplied by their operating voltage governs efficiency. The fill factor benefits from a minimal series resistance (R_S) and a maximum shunt resistance (R_{SH}). MPP, maximum power point; OC, open circuit; SC, short circuit. **c,** The solar spectrum is broadband, evenly dispersed across visible and infrared components. The optimal single-junction solar cell has a bandgap that corresponds to 950–1,250 nm. **d,** The theoretical efficiency of solar cells can be improved by sequentially harvesting the Sun's constituent spectral components in tandem, using multijunction cells that reduce losses associated with intraband relaxation.

quicker than recombination, achieving near-unity net collection of photogenerated electrons[18].

Impedance spectroscopy is an important tool for investigating electron transport and recombination in mesoscopic titanium-dioxide films, as well as interfacial charge transfer at the counter electrode and diffusion in the electrolyte. The shapes of the frequency-dependent impedance response curves allow clear identification of each of these processes. By using a transmission line model[19], electrical cell parameters, such as the resistances for electron diffusion and recombination, the chemical capacitance of the films, the diffusion coefficient of the redox mediator in the electrolyte, the resistance for electron transfer at the counter electrode and the series resistance of the cells can be extracted. Impedance parameters show the energetic distribution of the localized states in the bandgap of the oxide nanoparticles. Electrons move between the trap states and the conduction band, and only free electrons contribute to the steady-state diffusion process. The dependence of the recombination resistance on the bias potential follows an

exponential function, suggesting a trap state-mediated charge-transfer mechanism. The width of the energy distribution of trap states can be quantified, and a prevalence of shallow traps, for a given open-circuit voltage, can increase the maximum extractable power from the cell, or fill factor[20]. Progress is still needed to quantify accurately the charge-carrier diffusion length[21], and to apply impedance spectroscopy to solid-state sensitized heterojunction solar cells[22] and colloidal quantum-dot sensitized solar cells[23].

Understanding and controlling the energetics of the charge-separating interface has contributed to the rapid improvement of colloidal quantum-dot solar cells. Early advances in performance relied on a metal-semiconductor Schottky junction, in which a light metal with a shallow work function established a charge-separating electric field within the p-type colloidal quantum-dot solid[24]. This model system was easily fabricated, rapidly achieved a multi-per-cent level of performance[25], and resulted in the rapid accrual of knowledge of doping and the establishment of charge-carrier drift and diffusion regions in colloidal quantum-dot solids[26].

Depleted heterojunction colloidal quantum-dot devices[27] (Fig. 3b) have a number of advantages over Schottky architecture. Separating charges on the light-absorbing side of the device lessened the reliance on long-distance transport within the quantum-dot film. The n-type titanium-oxide to p-type colloidal quantum-dot film heterojunction removed the limits on open-circuit voltage that arose as a result of Fermi-level pinning in Schottky devices. The barrier-to-hole extraction presented by the large-bandgap titanium dioxide was used to prevent back recombination.

The electron affinity of the acceptor that makes up the depleted heterojunction has also been systematically varied[28]. Cyclic voltammetry studies of electrode and quantum-dot materials showed that only a mildly favourable band offset was required to allow efficient charge injection into the titanium dioxide. This is consistent with the small binding energy of electron–hole pairs in metal chalcogenides, and with the p–n junction also driving carrier extraction along with the hetero-structure band offset[29]. Multilayer electrodes in colloidal quantum-dot solar cells have been exploited to allow greater freedom in the joint optimization of doping and band offset[30].

Inorganic solution-processed solar cells, such as those based on CIGS and CZTS, are also reliant on the front junction for efficient charge separation. Here an n-type semiconductor, such as cadmium sulphide, forms a depletion region when in contact with the p-type absorber. A large positive conduction band offset (spike) (Fig. 3d) presents a barrier for minority carrier (electron) collection, reducing short-circuit current. By contrast, negative offset (cliff) leads to increased recombination at the buffer–absorber interface, thereby reducing open-circuit voltage. Ideally, the device would have a small 0–0.4 eV conduction-band offset spike, as found in copper-indium-gallium-sulphur-selenide (CIGSSe) devices employing a cadmium-sulphide buffer[31,32]. Efforts to replace cadmium sulphide with a buffer that contains no heavy metals must take into account the effect of conduction-band offset on device performance[33].

At the back of the CIGS or CZTS devices, an ohmic contact is required to collect majority carriers from the absorber. Molybdenum provides an ohmic contact for both CIGSSe and copper-zinc-tin-sulphur-selenium (CZTSSe) devices, as a result of the molybdenum-selenide interfacial layer that forms between the two, during high-temperature thermal processing[34]. Not only does the molybdenum act as a back contact, but it also provides a partial chemical barrier. Trace amounts of sodium significantly improve CIGSSe device performance[35], particularly open-circuit voltage, and this element is often introduced by fabricating devices on soda-lime glass. The flow of sodium into the absorber can be controlled during device fabrication by choosing a particular molybdenum-film thickness, density or grain structure, as well as through the application of a diffusion barrier to the glass.

In organic solar cells, the charge-transfer state is formed during rapid (about 40 fs)[36] exciton dissociation[37,38] at organic semiconductor

heterojunctions. The energy of the charge-transfer state has an important role in determining the open-circuit voltage of the cell. The rapidly ensuing dissociation into free charge carriers, which must out-pace recombination, maximizes the short-circuit current. Maximizing open-circuit voltage requires organic or polymer heterojunctions in which the energy of the lowest intramolecular singlet excitons in the donor and acceptor is just sufficient to create the charge-transfer state, placing the system at the threshold for photovoltaic operation: synthetically this requires careful tuning of the highest occupied molecular orbital (HOMO) and LUMO levels to maximize the open-circuit voltage while still achieving efficient charge separation. Detailed photophysical studies have quantified the considerable difference in binding energy of charge-transfer excitons compared with bulk-charge separation[39], and indicate the importance of work aimed at directing charge flow away from the heterojunction to avoid losses as a result of bound charge-transfer excitons.

The electronic properties of the donor–acceptor interface in organic bulk heterojunction solar cells have been analysed using a combination of highly sensitive photothermal deflection spectroscopy, external quantum efficiency measurements and electroluminescence spectroscopy to obtain detailed information on the energy and role of the interfacial charge-transfer state in generating free charges[38,40]. Scanning tunnelling microscopy and spectroscopy probed the local photovoltaic performance of prototypical polymer–fullerene bulk heterojunction films with 10-nm resolution. Fullerene-rich clusters act as sinks, extracting electrons from an interface layer of a homogeneously mixed polymer–fullerene matrix, surrounding the fullerene cluster and allowing quantitative correlation between nanoscopic and macroscopic device photovoltaic performance[41].

As well as the donor–acceptor junction, the interface of the photoactive layer with the electrodes is important for the operation of organic solar cells. Once the HOMO and LUMO levels have been optimized inside the device, the difference in the work function of the electrodes can limit the maximum attainable open-circuit voltage. By incorporating thin interfacial layers of either alcohol- or water-soluble polymers[42] or a fullerene bisadduct surfactant[43] between the photoactive layer and the electron-collecting electrode, performance was substantially increased. These improvements have been attributed to the formation of dipole layers and to Fermi-level pinning, respectively. At the hole-collecting electrode, replacement of the standard electrode material, poly-3,4-ethylenedioxy-thiophene–poly(styrene sulphonate) (PEDOT–PSS), with nickel oxide (ref. 44) or a single layer of electronically tuned graphene oxide[45], has also resulted in significant improvements. Further research is crucial to develop solution-processed tandem and multijunction polymer bulk-heterojunction solar cells in which the individual subcells are stacked using optically transparent electrically conducting recombination layers[46,47].

Interfaces within the absorber

Much of the progress in colloidal quantum-dot photovoltaics has occurred within the quantum-dot solid itself, which has a large interfacial area. Early work in quantum-dot photovoltaics[48] assumed that a two-phase solution, similar to the bulk heterojunction of organic photovoltaics, could extend the excited state lifetimes. However, completely removing the polymer phase and organic insulating ligands led to marked improvements in transport performance[49], ensuring the focus was on essentially pure colloidal quantum-dot films. Only the shortest organic ligands were retained for surface passivation. Solution-phase exchange to short organic linkers — such as butylamine — took colloids to the edge of stability in non-polar solvents, and allowed sufficient communication among the nanoparticles to achieve efficient extraction over 100-nm length scales[25]. Solid-state exchanges were devised[50] in which a quantum-dot film is cast, and a crosslinking agent is introduced into a solvent that does not redisperse the solid-state quantum-dot film, but instead aids in the displacement and removal of the original ligands[24]. The organic molecule chosen plays an important
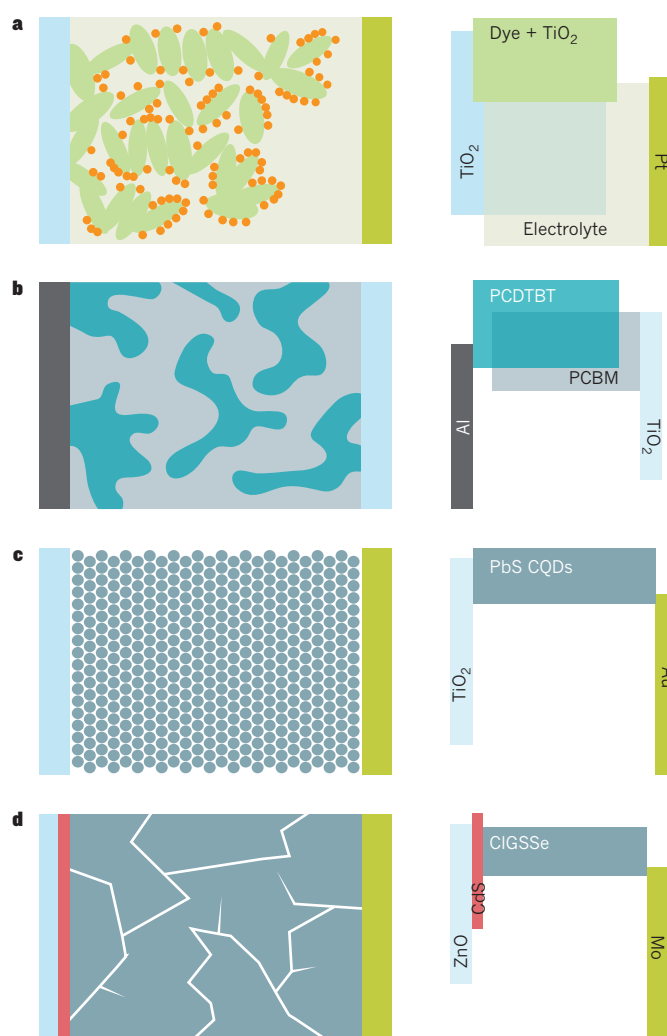

Figure 3 | Solution-processed solar cell architectures. a, In the dye-sensitized solar cell, light-absorbing dye (orange circles) is tethered to an electron-accepting three-dimensional electrode. The dye injects an excited photoelectron into the electrode and is recharged through an infiltrated electrolyte. **b**, The excitons generated in the light absorber of organic solar cells that benefit from an interpenetrating bulk heterojunction, rapidly diffuse to an interface where they are separated. This allows charge extraction prior to recombination. **c**, The light-absorbing region of colloidal quantum-dot solar cells consists of a densely-packed, well-passivated collection of monodispersed semiconductor nanoparticles that have a size-tuned bandgap. The quantum-dot layer transfers electrons to the titanium-dioxide electrode and transports holes to the back ohmic contact. **d**, The minority carriers in inorganic bulk polycrystalline solar cells diffuse through a polycrystalline semiconductor to be extracted at a heterojunction. The panels on the left illustrate the three-dimensional physical structure of the cells, the panels on the right show the flat band (open circuit) energetic structure of the cells.

part in establishing the film morphology, and the thiol-end functional group has been particularly effective in terminating nanoparticle surface dangling bonds[51]. The conductivity of the linker molecule itself may be important in enhancing transport in colloidal quantum-dot solids[13].

Because of the intense focus on inorganic semiconductor nanoparticles capped using organic ligands, enhanced passivation and retained quantum confinement using an inorganic passivation strategy came as a surprise[52]. Time-resolved transient infrared spectroscopy (Fig. 4e) indicated there was a crucial role for trap states, as opposed to the quantum-confined core levels, in determining the effectiveness of transport in colloidal quantum-dot films[52,53]. Halide anions introduced during solid-state film treatments have led to a marked reduction in the density of trap states deep within the bandgap of the colloidal quantum-dot solid.

This insight has been extended to the organic passivation domain, in which the mechanisms that underlie improved performance associated with optimal ligand selections have been traced directly to the quality of passivation in the final quantum-dot solid[53]. Optical field-effect transistor studies[54] of colloidal quantum-dot films have also suggested a midgap band. The work connects the relationship between dark transport and photoconductivity in films of lead-sulphide nanocrystals. Spectrally resolved photoresponses of these devices show that a weakly conductive midgap band is responsible for charge transport in the dark. When illuminated, the material becomes dominated by band-edge quantized states. The midgap band is important even under illumination because its occupancy controls the dynamics of band-edge charges. The colloidal quantum-dot field will benefit from studies that help to find, and explain, the relationships between electron and hole mobilities measured using field-effect transistors, time of flight, and charge extraction, by linearly increasing voltage techniques.

Solution-processed CIGSSe or CZTSSe devices also provides examples of chemical and interfacial effects within the semiconductor itself. Processing of thin-film chalcogenide compounds from ink-like solutions using techniques such as spin coating, slit casting and spray coating can control the metal stoichiometry, which is crucial for high device performance[55]. In CIGSSe devices, the indium to gallium ratio is used to tailor the bandgap, and the materials should be copper-deficient relative to the ideal chalcopyrite stoichiometry to avoid detrimental electrical shunting. Similarly in CZTSSe devices, films should be both copper-poor and zinc-rich to form the highest-performing devices[56]. Using solution-based approaches, the final metal composition can be determined from the initial quantities of the elements in the solution; although for CZTSSe devices, tin volatility and loss during thermal processing must be mitigated to achieve the highest performance[57]. For CIGSSe, the ease with which targeted impurities can be introduced into the deposition solution led to the discovery that low levels of antimony markedly improved grain structure and CIGSSe device performance[58] (Fig. 4c).

High performance relies on diffusion during CIGSSe or CZTSSe device processing, and homogeneity in the final film. In addition to sodium diffusing from the glass substrate[35], cadmium diffuses into the absorber to a depth of about 10 nm during cadmium-sulphide chemical bath deposition (studied mostly in CIGSSe devices), leading to n-type doping (Cd_{Cu} donor defects) that can invert the top layer of the absorber and increase the band bending, and hence electric field, near the semiconductor junction[59]. Deeper diffusion of cadmium has been reported in films with many grain boundaries — the internal interfaces within the absorber film[60].
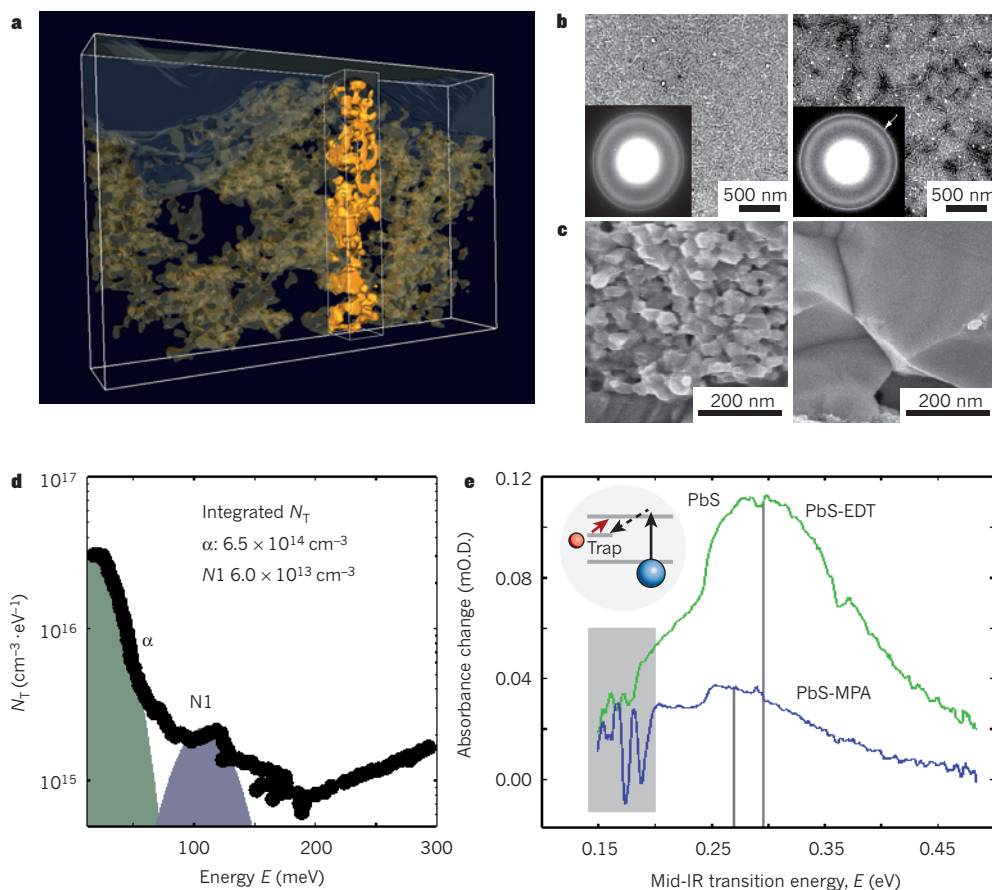

Figure 4 | Analysis of interface morphology and electronic properties.
a, Three-dimensional electron tomography maps the detailed structure of bulk heterojunctions and guides optoelectronic modelling (Reprinted with permission from ref. 12). **b**, In the formation of a phenyl-C61-butyric acid methyl ester–poly(3-hexylthiophene) (PCBM) heterojunction, annealing conditions (right panel) control the length scale of interpenetration of the donor and acceptor materials (Reprinted with permission from ref. 11). **c**, Scanning electron microscope images of copper-indium-gallium-selenide (CIGS) semiconductors prepared with (right panel) or without a small concentration of antimony (Sb). Antimony improved the grain structure achieved in film processing (Reprinted with permission from ref. 58). **d**, Admittance spectroscopy shows the trap states in solution-processed CIGS devices. By correlating with materials analysis, materials chemistry mechanisms that underlie recombination centre formation could be pinpointed (Reprinted with permission from ref. 64). N_T, defect density of states; α, trap levels with activation energies at around 25 meV (green area); $N1$, trap levels with activation energies at around 110 meV (purple area). **e**, Colloidal quantum-dot solar cells have, until recently, relied mainly on organic molecule-based control over surface passivation. A highly compact halogen-based inorganic passivation strategy superseded the performance of the organic approach. Time-resolved infrared spectroscopy was used to explore how organic and inorganic ligands used in the passivation of colloidal quantum-dot solids affect electronic trap states (Reprinted with permission from ref. 53). EDT, ethane dithiol; IR, infrared; MPA, 3-mercaptopropionic acid; PbS, lead sulphide.

Grain boundaries are typically copper-poor in CIGSSe devices[61] relative to the grain interiors, which modifies the valence band offset such that the boundaries repel holes and recombination is reduced. Low-temperature air-annealing after device fabrication improves the performance of CIGSSe and CZTSSe devices, particularly for those with small grain size, as a result of grain-boundary passivation[62]. Finally, in the bulk absorber at the atomic scale, elemental vacancy and substitutional defects, such as V_{Cu}, In_{Cu} and Cu_{Zn}, significantly affect doping and recombination, and consequently device performance[63,64].

Trap spectroscopies have been used in solution-processed inorganic solar cells and have been combined with a suite of advanced-materials analysis methods[64,65]. The defect level distribution for solution-processed CIGSSe films grown with low selenium supply showed trap levels with activation energies of 25 meV and 110 meV (ref. 66) using admittance spectroscopy (Fig. 4d). Materials analysis has shown the importance of control over the supply of selenium during CIGSSe grain growth. The difference in selenium supply has a negligible effect on CIGSSe grain structures, crystal orientation and bulk composition, when measured by cross-section scanning electron microscopy or TEM, X-ray diffraction and secondary ion mass spectrometry. But when selenium supply is insufficient, a defective chalcopyrite layer with a high density of $(In,Ga)_{Cu}$ defects forms near the CIGSSe surface owing to the loss of selenium from the CIGSSe lattice. This defective chalcopyrite layer leads to more pronounced rollover and crossover signatures in J–V curves. The occupation of existing V_{Cu} by extra (In, Ga) atoms to form $(In, Ga)_{Cu}$ defects is also manifest in their defect spectra, in which a significant decrease in shallow acceptor defects (attributed to V_{Cu} defects) but an increase in the deeper $N1$ defect level (110 meV from the band edge) (attributed to $(In, Ga)_{Cu}$ defects) is observed. These defects affect solar cell performance by acting as Shockley–Read–Hall recombination centres. This insight can be used to further optimize CIGSSe processing, highlighting the importance of comprehensive electronic and materials characterization.

Spectral use to improve performance

In DSSCs, using co-sensitizers with black ruthenium dye has resulted in a power-conversion efficiency of 11.4% (ref. 67). A further increase in power-conversion efficiency to 12.3% has been reported[18]. This was achieved by using a judiciously engineered porphyrin sensitizer along with a cosensitizer and Tris(2,2′-bipyridyl)cobalt(III) as a redox shuttle[68] (Fig. 5). This redox shuttle yields substantially higher open-circuit voltage values than the iodide-based electrolyte. If validated by a photovoltaics calibration laboratory, the power-conversion efficiency would be the highest achieved for a DSSC under standard reporting conditions.

In organic photovoltaics, progress on small-bandgap polymers and small molecules has been chiefly responsible for achieving 8.4% efficiency in a single-junction low-bandgap polymer cell[42] and 8.6% in a tandem configuration[69]. Achieving these performance levels required synthesizing a small-energy-bandgap polymer (less than 1.5 eV) with carefully tuned HOMO and LUMO levels to maximize the open-circuit voltage, but still achieve efficient charge separation. Optimization of both charge-carrier mobility and fine-phase separation with the acceptor led to a high current density and fill factor. As yet undisclosed organic semiconductors have achieved record certified solar-cell efficiencies of 10.0% for single junctions[70] and 10.6% for tandem devices.

Efforts to improve colloidal quantum-dot solar photovoltaics are based on improved spectral use. The optimal single-junction bandgap close to a wavelength of roughly 1 μm is achieved using readily synthesized lead-sulphide quantum dots with about a 3-nm diameter. These devices have progressed rapidly from concept[48] to all-quantum-dot (polymer-free) devices based on Schottky junctions[13,25,71]. Depleted-heterojunction architectures[27] have achieved power-conversion efficiencies of 6% (ref. 52). The quantum-dot tandem cell is the first tandem to use the same material in both the large-bandgap front cell and small-bandgap back cell, with quantum-size-effect tuning alone allowing a wide variation in bandgaps (1.6 eV and 1.0 eV)[72]. This result relied on
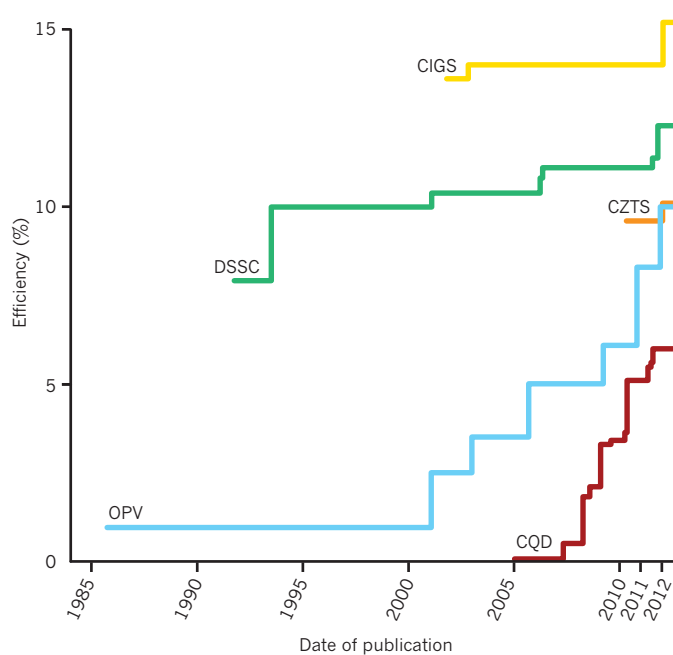

Figure 5 | Progress in solution-processed photovoltaic device performance. Organic solution-processed photovoltaic (OPV) cells were developed in the 1980s, since then their efficiency has increased and dye-sensitized solar cells (DSSCs), solution-processed inorganic solar cells (CZTS and CIGS) and colloidal quantum-dot (CQD) solar cells have been introduced. The figure includes representative significant performance advances for each technology family, recent reviews[1–4] contain comprehensive accounts of this progress.

an interconnection strategy known as the graded recombination layer, which employed a stepwise progression in work functions from the shallow-work-function electron acceptor of the back cell to the deep-work-function hole acceptor of the front cell.

CZTSSe and CIGSSe films control the bandgap by optimizing the sulphur to selenium ratio and metal substitution[73,74], which can further enhance spectral use and minimize recombination in this materials class.

Controlling heterointerfaces

The first organic photovoltaics devices were planar[75], but they soon progressed with the advent of the bicontinuous network of internal donor–acceptor heterojunctions[9] founded on rapid photoinduced electron transfer from the excited state of a semiconducting polymer onto C_{60} buckminsterfullerene. Refining the control over molecular morphology of the active layer[76,77] by improving process conditions had a principal role in increasing the power-conversion efficiency from a few per cent a decade ago[9] to more than 10% in 2012 (ref. 70). In colloidal quantum dots, both nanoparticle[15] and patterned-substrate electrodes[16] enhanced short-circuit currents by about 20%. In both cases, improved control over the aspect ratio (morphology), as well as transport and trapping, at these interfaces could provide further benefits.

Controlling the bulk semiconductor solid

Solution-based approaches provide good control over film stoichiometry. One of the first approaches for CIGSSe devices involved depositing metal-oxide nanoparticle-based precursors onto a substrate, chemically reducing the precursor film to the metals using an anneal in hydrogen, and subsequently selenizing or sulphurizing the film using a post-deposition treatment in a sulphur or selenium atmosphere[78], leading to CIGSSe devices with 13.6% efficiency. An analogous approach using chalcogenide-based nanoparticles subsequently improved efficiency to 14% (ref. 79). A pure-solution approach using hydrazine as the solvent led to 15.2% efficiency[80] for a fully solution-processed device, closing the performance gap with vacuum-deposited devices, which have a

20.3% efficiency. A similar hydrazine-based slurry approach for the CZTSSe system led to 10.1% efficiency, which is the highest achieved by any solution- or vacuum-based approach for this materials system, demonstrating the potential of solution-processed devices to compete with vacuum-based analogues in performance[81]. Analogous progress using a pure-nanoparticle approach — not requiring hydrazine — has led to an 8% efficient cell[74]. Stoichiometry and its control are essential to CZTSSe, and depositing material is complicated by the narrow range of phase stability, and its susceptibility to the loss of tin, sulphur and selenium during heat treatment[57].

The success of the hydrazine-based approach for CIGSSe and CZTSSe devices is as a result of the nanoscale mixing of the various constituents in the precursor film. Metal species already have the desired metal-chalcogen bonding, and incorporating excess sulphur or selenium in the film before heat treatment allows the rapid formation and crystallization of the CIGSSe or CZTSSe phase. Clean decomposition and dissociation of hydrazine from the precursor film during heat treatment also contributes to the formation of an impurity-free (especially oxygen and carbon) final film.

Outlook

Solution-processed solar cells are a promising technology for reaching 15% solar-power-conversion efficiency and beyond in low-cost, flexible solar modules. Inorganic solution-processed bulk semiconductor approaches have a tried-and-tested solar-materials composition achieved not through more costly physical deposition methods, but instead through solution-phase processing. Reducing the cost and complexity of solvents, their handling during processing and the temperature required in thermal processing are all being investigated. Organic solar cells and DSSCs have efficiencies in excess of 10%, and each has continued to progress in performance and reliability; for example, DSSC modules with 8% efficiency have passed tests for the outdoor use of photovoltaic panels, including long-term exposure to heat and humidity, light soaking and temperature cycling[82]. Life-cycle analysis suggests that the energy payback for a DSSC is less than one year in a southern European climate, compared with more than three years for silicon solar cells. The youngest of the technologies reviewed, colloidal quantum-dot solar cells, raises the possible performance further in view of their intrinsic compatibility with systematically engineered multijunction architectures, and the possible opportunity to exploit multi-exciton generation[83]. These materials require further improvements in transport and passivation to approach their full potential.

Improvements in efficiency will include addressing the open-circuit voltage deficit in solution-processed solar technologies, especially CZTSSe devices. The voltage provided by many solution-processed devices is appreciably lower than the theoretical maximum. In CZTSSe devices, the voltage seems to be limited by interface-dominated recombination[84]. Understanding the origins of this process requires a deeper understanding of the materials interfaces. In organic photovoltaics, at present, the open-circuit voltage is over 0.6 eV smaller than the bandgap[85], but in principle a difference as little as 0.35 eV is possible. Reducing the energy losses associated with exciton dissociation, charge separation and collection will be essential.

Reducing ohmic losses must be achieved in many solution-processed device classes. A higher series resistance in CZTSSe devices than in CIGSSe devices (especially for high-sulphur-content absorber layers) and an increase in series resistance with reduced temperature, suggests the presence of an energetic barrier to charge-carrier extraction, or that CZTSSe devices have a deeper acceptor than CIGSSe devices[62], leading to carrier freeze-out at low temperatures. If a barrier to current transport is present, it must be located at the back contact, the charge-separating interface or at interfaces of the polycrystalline grains that make up the solid, and remedied.

In colloidal quantum-dot photovoltaics, work is needed to enhance passivation within the bandgap of the quantum-dot solid, in which midgap and shallow traps of considerable energetic depth below the quantum-confined band edges are present. Modelling indicates that trap-free quantum dots are, in principle, possible[86]. Shallow traps originate because of surface disorder and reconstructions, whereas deep traps form because of significantly undercoordinated atoms on the surface[87–89]. These effects are analogous to the exponential decay that can occur near the band edge, known as Urbach tails, owing to deviations of bond lengths and bond angles, from ideal bulk values and unsaturated dangling bonds, respectively. Satisfying the charge-neutral conditions when selecting the intended stoichiometry of the quantum dots — similar to electron counting rules that describe the reconstruction of flat surfaces — offers a maximum opening of the quantum-dot bandgap[86]. Surface self-healing to remove dangling bonds reduces the total energy of the dots further[87]. These findings suggest that the dots have an intrinsic propensity to be trap-free in thermodynamic equilibrium conditions. In contrast, experimental work has used synthesis and ligand-exchange conditions that are highly non-equilibrium and kinetically driven, requiring a renewed effort in thermodynamically driven synthesis and exchange.

Progress in the control of structured interfaces is ongoing for photovoltaics that can benefit from high-surface-area charge-separating junctions. Mesostructures for enhanced light-harvesting are a particularly fertile opportunity, including nanorods composed of oxides with a core shell structure, gyroids and nanochannel-based mesoporous semiconductor oxide beads. These will facilitate electron transport and collection, and increase multiple light scattering, leading to an augmented optical path for a given amount of the light-absorbing moiety.

Improving the control of structured interfaces allows the introduction of light management techniques. In addition to random surface texturing of the electrode-absorber interfaces used in conventional solar cells to enhance absorption through multiple-angle scattering[90], photonic and plasmonic mesostructures can be incorporated into thin-film devices to increase the effective optical path lengths[91]. Examples are sub-wavelength metal nanoparticles, grating patterned metal films, semiconductor nanowires and photonic crystals[92]. Photocurrent enhancements of 33% have been demonstrated for thin-film plasmonic silicon devices[93]. Initial studies in plasmonic organic cells[94] and DSSCs[95] have resulted in efficiency enhancements of 20% and 50–100%, respectively, which are promising for light trapping in solution-processed technologies.

One opportunity for the field of solution-processed photovoltaics is to combine concepts and materials from diverse materials communities. For example, quantum dots could be used as replacements for chromophores in DSSCs, with a monolayer of size-tuned nanoparticles forming the broad spectral reach of semiconductors, and complemented by the well-understood charge transfer and back recombination blocking of the DSSC architecture. With their excellent efficiency in harvesting the visible portion of the Sun's spectrum, organic photovoltaics could be integrated with infrared-bandgap semiconductors[96], such as colloidal quantum-dot solids, as the back cell in tandem or multijunction designs. While these various opportunities and challenges are addressed, solution-processed photovoltaics will continue to help drive higher performance at lower cost for the widespread deployment of solar-harvesting technology. ∎

1. Nazeeruddin, M. K., Baranoff, E. & Grätzel, M. Dye-sensitized solar cells: a brief overview. *Solar Energy* **85,** 1172–1178 (2011).
    This article provides a review of DSSCs.
2. Nelson, J. Polymer: fullerene bulk heterojunction solar cells. *Mater. Today* **14,** 462–470 (2011).
    This review is an overview of organic and polymer solar cells.
3. Todorov, T. & Mitzi, D. B. Direct liquid coating of chalcopyrite light absorbing layers for photovoltaic devices. *Eur. J. Inorg. Chem.* **2010,** 17–28 (2010).
    This article reviews inorganic solution-processed solar cells.
4. Sargent, E. H. Colloidal quantum dot solar cells. *Nature Photon* **6,** 133–135 (2012).
    This article is a recent review of colloidal quantum-dot solar cells.
5. Shockley, W. & Queisser, H. J. Detailed balance limit of efficiency of p-n junction solar cells. *J. Appl. Phys.* **32,** 510–519 (1961).
6. O'Regan, B. & Grätzel, M. A low-cost, high-efficiency solar cell based on dye-sensitized colloidal TiO$_2$ films. *Nature* **353,** 737–740 (1991).

This is a seminal paper on DSSCs, reporting an early major advance in performance.

7. Grätzel, M. Recent advances in sensitized mesoscopic solar cells. *Acc. Chem. Res.* **42,** 1788–1798 (2009).

8. Shaheen, S. E. *et al.* 2.5% efficient organic plastic solar cells. *Appl. Phys. Lett.* **78,** 841843 (2001).
   This is the first report of a bulk heterojunction used in organic polymer solar cells.

9. Yu, G., Gao, J., Hummelen, J. C., Wudl, F. & Heeger, A. J. Polymer photovoltaic cells: enhanced efficiencies *via* a network of internal donor-acceptor heterojunctions. *Science* **270,** 1789–1791 (1995).
   This is a seminal paper on polymer photovoltaics, reporting the benefits to be achieved at the bulk heterojunction.

10. Maturová, K., van Bavel, S. S., Wienk, M. M., Janssen, R. A. J. & Kemerink, M. Description of the morphology dependent charge transport and performance of polymer:fullerene bulk heterojunction solar cells. *Adv. Funct. Mater.* **21,** 261–269 (2011).

11. Yang, X. *et al.* Nanoscale morphology of high-performance polymer solar cells. *Nano Lett.* **5,** 579–583 (2005).

12. Oosterhout, S. D. *et al.* The effect of three-dimensional morphology on the efficiency of hybrid polymer solar cells. *Nature Mater.* **8,** 818–824 (2009).
    This article is an in-depth investigation of how interface morphology affects polymer solar-cell performance.

13. Koleilat, G. I. *et al.* Efficient, stable infrared photovoltaics based on solution-cast colloidal quantum dots. *ACS Nano* **2,** 833–840 (2008).

14. Clifford, J. P. *et al.* Fast, sensitive and spectrally tuneable colloidal-quantum-dot photodetectors. *Nature Nanotechnol.* **4,** 40–44 (2009).

15. Barkhouse, D. A. R. *et al.* Depleted bulk heterojunction colloidal quantum dot photovoltaics. *Adv. Mater.* **23,** 3134–3138 (2011).

16. Kramer, I. J. *et al.* Ordered nanopillar structured electrodes for depleted bulk heterojunction colloidal quantum dot solar cells. *Adv. Mater.* **24,** 2315–2319 (2012).

17. Persson, P., Lundqvist, M. J., Ernstorfer, R., Goddard, W. A. III & Willig, F. Quantum chemical calculations of the influence of anchor-cum-spacer groups on femtosecond electron transfer times in dye-sensitized semiconductor nanocrystals. *J. Chem. Theory Comput.* **2,** 441–451 (2006).

18. Yella, A. *et al.* Porphyrin-sensitized solar cells with cobalt (II/III)-based redox electrolyte exceed 12 percent efficiency. *Science* **334,** 629–634 (2011).

19. Bisquert, J. Theory of the impedance of electron diffusion and recombination in a thin layer. *J. Phys. Chem. B* **106,** 325–333 (2001).

20. Wang, Q. *et al.* Characteristics of high efficiency dye-sensitized solar cells. *J. Phys. Chem. B* **110,** 25210–25221 (2006).

21. Villanueva-Cab, J., Wang, H., Oskam, G. & Peter, L. M. Electron diffusion and back reaction in dye-sensitized solar cells: the effect of nonlinear recombination kinetics. *J. Phys. Chem. Lett.* **1,** 748–751 (2010).

22. Fabregat-Santiago, F. *et al.* Electron transport and recombination in solid-state dye solar cell with spiro-OMeTAD as hole conductor. *J. Am. Chem. Soc.* **131,** 558–562 (2009).

23. Mora-Seró, I. *et al.* Recombination in quantum dot sensitized solar cells. *Acc. Chem. Res.* **42,** 1848–1857 (2009).

24. Klem, E. J. D., MacNeil, D. D., Cyr, P. W., Levina, L. & Sargent, E. H. Efficient solution-processed infrared photovoltaic cells: planarized all-inorganic bulk heterojunction devices via inter-quantum-dot bridging during growth from solution. *Appl. Phys. Lett.* **90,** 183113 (2007).

25. Johnston, K. W. *et al.* Schottky-quantum dot photovoltaics for efficient infrared power conversion. *Appl. Phys. Lett.* **92,** 151115 (2008).

26. Johnston, K. W. *et al.* Efficient Schottky-quantum-dot photovoltaics: the roles of depletion, drift, and diffusion. *Appl. Phys. Lett.* **92,** 122111 (2008).

27. Pattantyus-Abraham, A. G. *et al.* Depleted-heterojunction colloidal quantum dot solar cells. *ACS Nano* **4,** 3374–3380 (2010).
    This article reports the first colloidal quantum-dot solar cell to exceed 5% solar power conversion efficiency and the architecture that has allowed its subsequent advances.

28. Liu, H. *et al.* Electron acceptor materials engineering in colloidal quantum dot solar cells. *Adv. Mater.* **23,** 3832–3837 (2011).

29. Hyun, B. R. *et al.* Electron injection from colloidal PbS quantum dots into titanium dioxide nanoparticles. *ACS Nano* **2,** 2206–2212 (2008).

30. Koleilat, G. I. *et al.* A donor-supply electrode (DSE) for colloidal quantum dot photovoltaics. *Nano Lett.* **11,** 5173–5178 (2011).

31. Minemoto, T. *et al.* Cu(In,Ga)Se$_2$ solar cells with controlled conduction band offset of window/Cu(In,Ga)Se$_2$ layers. *J. Appl. Phys.* **89,** 8327–8330 (2001).

32. Haight, R. *et al.* Band alignment at the Cu$_2$ ZnSn (S$_x$Se$_{1-x}$)$_4$ /CdS interface. *Appl. Phys. Lett.* **98,** 253502 (2011).

33. Barkhouse, D. A. R. *et al.* Cd-free buffer layer materials on Cu$_2$ZnSn(S$_x$Se$_{1-x}$)$_4$: Band alignments with ZnO, ZnS, and In$_2$S$_3$. *Appl. Phys. Lett.* **100,** 193904–193905 (2012).

34. Wada, T., Kohara, N., Nishiwaki, S. & Negami, T. Characterization of the Cu(In,Ga)Se$_2$/Mo interface in CIGS solar cells. *Thin Solid Films* **387,** 118–122 (2001).

35. Rockett, A. The effect of Na in polycrystalline and epitaxial single-crystal CuIn$_{1-x}$Ga$_x$Se$_2$. *Thin Solid Films* **480–481,** 2–7 (2005).

36. Brabec, C. J. *et al.* Tracing photoinduced electron transfer process in conjugated polymer/fullerene bulk heterojunctions in real time. *Chem. Phys. Lett.* **340,** 232–236 (2001).

37. Veldman, D. *et al.* Compositional and electric field dependence of the dissociation of charge transfer excitons in alternating polyfluorene copolymer/fullerene blends. *J. Am. Chem. Soc.* **130,** 7721–7735 (2008).

38. Vandewal, K., Tvingstedt, K., Gadisa, A., Inganäs, O. & Manca, J. V. On the origin of the open-circuit voltage of polymer-fullerene solar cells. *Nature Mater.* **8,** 904–909 (2009).

39. Gélinas, S. *et al.* The binding energy of charge-transfer excitons localized at polymeric semiconductor heterojunctions. *J. Phys. Chem. C* **115,** 7114–7119 (2011).

40. Lee, J. *et al.* Charge transfer state versus hot exciton dissociation in polymer-fullerene blended solar cells. *J. Am. Chem. Soc.* **132,** 11878–11880 (2010).

41. Maturová, K., Janssen, R. A. J. & Kemerink, M. Connecting scanning tunneling spectroscopy to device performance for polymer:fullerene organic solar cells. *ACS Nano* **4,** 1385–1392 (2010).

42. He, Z. *et al.* Simultaneous enhancement of open-circuit voltage, short-circuit current density, and fill factor in polymer solar cells. *Adv. Mater.* **23,** 4636–4643 (2011).

43. O'Malley, K. M., Li, C.-Z., Yip, H.-L. & Jen, A. K. Y. Enhanced open-circuit voltage in high performance polymer/fullerene bulk-heterojunction solar cells by cathode modification with a C$_{60}$ surfactant. *Adv. Energy Mater.* **2,** 82–86 (2012).

44. Irwin, M. D., Buchholz, D. B., Hains, A. W., Chang, R. P. H. & Marks, T. J. p-Type semiconducting nickel oxide as an efficiency-enhancing anode interfacial layer in polymer bulk-heterojunction solar cells. *Proc. Natl Acad. Sci. USA* **105,** 2783–2787 (2008).

45. Murray, I. P. *et al.* Graphene oxide interlayers for robust, high-efficiency organic photovoltaics. *J. Phys. Chem. Lett.* **2,** 3006–3012 (2011).

46. Gilot, J., Wienk, M. M. & Janssen, R. A. J. Double and triple junction polymer solar cells processed from solution. *Appl. Phys. Lett.* **90,** 143512 (2007).

47. Jin, Y. K. *et al.* Efficient tandem polymer solar cells fabricated by all-solution processing. *Science* **317,** 222–225 (2007).

48. McDonald, S. A. *et al.* Solution-processed PbS quantum dot infrared photodetectors and photovoltaics. *Nature Mater.* **4,** 138–142 (2005).

49. Konstantatos, G. *et al.* Ultrasensitive solution-cast quantum dot photodetectors. *Nature* **442,** 180–183 (2006).

50. Konstantatos, G., Clifford, J., Levina, L. & Sargent, E. H. Sensitive solution-processed visible-wavelength photodetectors. *Nature Photonics* **1,** 531–534 (2007).

51. Barkhouse, D. A. R., Pattantyus-Abraham, A. G., Levina, L. & Sargent, E. H. Thiols passivate recombination centers in colloidal quantum dots leading to enhanced photovoltaic device efficiency. *ACS Nano* **2,** 2356–2362 (2008).

52. Tang, J. *et al.* Colloidal-quantum-dot photovoltaics using atomic-ligand passivation. *Nature Mater.* **10,** 765–771 (2011).

53. Jeong, K. S. *et al.* Enhanced mobility-lifetime products in PbS colloidal quantum dot photovoltaics. *ACS Nano* **6,** 89–99 (2012).

54. Nagpal, P. & Klimov, V. I. Role of mid-gap states in charge transport and photoconductivity in semiconductor nanocrystal films. *Nature Commun.* **2,** 486, http://dx.doi.org/10.1038/ncomms1492 (2011).

55. Hibberd, C. J. *et al.* Non-vacuum methods for formation of Cu(In, Ga) (Se, S)$_2$ thin film photovoltaic absorbers. *Prog. Photovolt. Res. Appl.* **18,** 434–452 (2010).

56. Katagiri, H. *et al.* Development of CZTS-based thin film solar cells. *Thin Solid Films* **517,** 2455–2460 (2009).

57. Scragg, J. J., Ericson, T., Kubart, T., Edoff, M. & Platzer-Björkman, C. Chemical insights into the instability of Cu$_2$ZnSnS$_4$ films during annealing. *Chem. Mater.* **23,** 4625–4633 (2011).

58. Yuan, M. *et al.* Antimony assisted low-temperature processing of CuIn$_{1-x}$Ga$_x$Se$_{2-y}$S$_y$ solar cells. *Thin Solid Films* **519,** 852–856 (2010).

59. Liao, D. & Rockett, A. Cd doping at the CuInSe$_2$/CdS heterojunction. *J. Appl. Phys.* **93,** 9380–9382 (2003).

60. Rusu, M. *et al.* Three-dimensional structure of the buffer/absorber interface in CdS/ CuGaSe$_2$ based thin film solar cells. *Appl. Phys. Lett.* **95,** 173502 (2009).

61. Hetzer, M. J. *et al.* Direct observation of copper depletion and potential changes at copper indium gallium diselenide grain boundaries. *Appl. Phys. Lett.* **86,** 162105 (2005).

62. Mitzi, D. B. *et al.* Hydrazine-based deposition route for device-quality CIGS films. *Thin Solid Films* **517,** 2158–2162 (2009).

63. Chen, S., Gong, X. G., Walsh, A. & Wei, S. H. Defect physics of the kesterite thin-film solar cell absorber Cu$_2$ZnSnS$_4$. *Appl. Phys. Lett.* **96,** 021902 (2010).

64. Cao, Q. *et al.* Defects in Cu(In,Ga)Se$_2$ chalcopyrite semiconductors: a comparative study of material properties, defect states, and photovoltaic performance. *Adv. Energy Mater.* **1,** 845–853 (2011).

65. Guha, S. *et al.* Structural, defect, and device behavior of hydrogenated amorphous Si near and above the onset of microcrystallinity. *Appl. Phys. Lett.* **74,** 1860–1862 (1999).

66. Heath, J. T., Cohen, J. D. & Shafarman, W. N. Bulk and metastable defects in CuIn$_{1-x}$Ga$_x$Se$_2$ thin films using drive-level capacitance profiling. *J. Appl. Phys.* **95,** 1000–1010 (2004).

67. Han, L. *et al.* High-efficiency dye-sensitized solar cell with a novel co-adsorbent. *Energy Environ. Sci.* **5,** 6057–6060 (2012).

68. Feldt, S. M. *et al.* Design of organic dyes and cobalt polypyridine redox mediators for high-efficiency dye-sensitized solar cells. *J. Am. Chem. Soc.* **132,** 16714–16724 (2010).

69. Dou, L. *et al.* Tandem polymer solar cells featuring a spectrally matched low-bandgap polymer. *Nature Photonics* **6,** 180–185 (2012).

70. Green, M. A., Emery, K., Hishikawa, Y., Warta, W. & Dunlop, E. D. Solar cell efficiency tables (version 39). *Prog. Photovolt. Res. Appl.* **20,** 12–20 (2012).

71. Luther, J. M. *et al.* Schottky solar cells based on colloidal nanocrystal films. *Nano Lett.* **8,** 3488–3492 (2008).

72. Wang, X. *et al.* Tandem colloidal quantum dot solar cells employing a graded

recombination layer. *Nature Photonics* **5**, 480–484 (2011).
This article reports the first optimized tandem cell to use quantum size tuning alone to achieve the desired bandgaps in the constituent junctions.

73. Todorov, T. K., Reuter, K. B. & Mitzi, D. B. High-efficiency solar cell with earth-abundant liquid-processed absorber. *Adv. Mater.* **22**, E156–E159 (2010).

74. Guo, Q., Ford, G. M., Hillhouse, H. W. & Agrawal, R. in *Proc. 37th IEEE Photovoltaic Specialist Conf.* 003522–003526. (IEEE, 2011).

75. Tang, C. W. Two-layer organic photovoltaic cell. *Appl. Phys. Lett.* **48**, 183–185 (1986).

76. Ma, W., Yang, C., Gong, X., Lee, K. & Heeger, A. J. Thermally stable, efficient polymer solar cells with nanoscale control of the interpenetrating network morphology. *Adv. Funct. Mater.* **15**, 1617–1622 (2005).

77. Park, S. H. *et al.* Bulk heterojunction solar cells with internal quantum efficiency approaching 100%. *Nature Photon.* **3**, 297–302 (2009).

78. Kapoor, V. K., Fisher, M. & Roe, R. *Mat. Res. Soc. Symp. Proc.* H261–H267 (Material Research Society, 2001).

79. Van Duren, J. K. J., Leidholm, C., Pudov, A., Robinson, M. R. & Roussillon, Y. *Materials Research Society Symp. Proc.* 259–268 (Material Research Society, 2002).

80. Todorov, T. K., Gunawan, O., Gokmen, T. & Mitzi, D. B. Solution-processed Cu(In,Ga)(S,Se)$_2$ absorber yielding a 15.2% efficient solar cell. *Prog. Photovolt. Res. Appl.* http://dx.doi.org/10.1002/pip.1253 (2012).

81. Barkhouse, D. A. R., Gunawan, O., Gokmen, T., Todorov, T. K. & Mitzi, D. B. Device characteristics of a 10.1% hydrazine-processed Cu$_2$ZnSn(Se,S)$_4$ solar cell. *Prog. Photovolt. Res. Appl.* **20**, 6–11 (2012).

82. Arakawa, H. Y. T., Okada, K., Matsui, K., Kitamura, T., Tanabe, N. Highly durable dye-sensitized solar cells. *Fujikura Tech. Rev.* **2009**, 55–59 (2009).

83. Semonin, O. E. *et al.* Peak external photocurrent quantum efficiency exceeding 100% via MEG in a quantum dot solar cell. *Science* **334**, 1530–1533 (2011).

84. Gunawan, O., Todorov, T. K. & Mitzi, D. B. Loss mechanisms in hydrazine-processed Cu$_2$ ZnSn (Se,S)$_4$ solar cells. *Appl. Phys. Lett.* **97**, 233506 (2010).

85. Veldman, D., Meskers, S. C. J. & Janssen, R. A. J. The energy of charge-transfer states in electron donor-acceptor blends: insight into the energy losses in organic solar cells. *Adv. Funct. Mater.* **19**, 1939–1948 (2009).

86. Voznyy, O. Mobile surface traps in CdSe nanocrystals with carboxylic acid ligands. *J. Phys. Chem. C* **115**, 15927–15932 (2011).

87. Puzder, A., Williamson, A. J., Gygi, F. & Galli, G. Self-healing of CdSe nanocrystals: first-principles calculations. *Phys. Rev. Lett.* **92**, 217401 (2004).

88. Yu, M. *et al.* First principles study of CdSe quantum dots: stability, surface unsaturations, and experimental validation. *Appl. Phys. Lett.* **88**, 231910 (2006).

89. Frenzel, J., Joswig, J. O., Sarkar, P., Seifert, G. & Springborg, M. The effects of organisation, embedding and surfactants on the properties of cadmium chalcogenide (CdS, CdSe and CdS/CdSe) semiconductor nanoparticles. *Eur. J. Inorg. Chem.* **2005**, 3585–3596 (2005).

90. Yablonovitch, E. & Cody, G. D. Intensity enhancement in textured optical sheets for solar cells. *IEEE Trans. Electron. Dev.* **29**, 300–305 (1982).

91. Atwater, H. A. & Polman, A. Plasmonics for improved photovoltaic devices. *Nature Mater.* **9**, 205–213 (2010).

92. Ferry, V. E. *et al.* Optimized spatial correlations for broadband light trapping nanopatterns in high efficiency ultrathin film a-Si:H solar cells. *Nano Lett.* **11**, 4239–4245 (2011).

93. Pillai, S., Catchpole, K. R., Trupke, T. & Green, M. A. Surface plasmon enhanced silicon solar cells. *J. Appl. Phys.* **101**, 093105 (2007).

94. Yang, J. *et al.* Plasmonic polymer tandem solar cell. *ACS Nano* **5**, 6210–6217 (2011).

95. Brown, M. D. *et al.* Plasmonic dye-sensitized solar cells using core-shell metal-insulator nanoparticles. *Nano Lett.* **11**, 438–445 (2011).

96. Klem, E. J. D. *et al.* Planar PbS quantum dot/C$_{60}$ heterojunction photovoltaic devices with 5.2% power conversion efficiency. *Appl. Phys. Lett.* **100**, 173109 (2012).